Dynamic properties of hydrogen-bonded networks in supercritical water

J. Martí
*Departament de Física i Enginyeria Nuclear, Universitat Politècnica de Catalunya, B5-206 Campus Nord, 08034 Barcelona, Catalonia, Spain**
and Department of Chemistry, University of California, Berkeley, California 94720-1460
(Received 24 March 1999; revised manuscript received 31 August 1999)

Dynamic properties of supercritical water at temperatures between 573 and 773 K and densities between 0.49 and 0.83 g/cm^3 have been investigated by molecular dynamics simulation and compared to states located on the vapor-liquid coexistence curve. A flexible simple point charge potential has been assumed for interactions in the subcritical states, whereas a reparameterization of that model has been performed to model the supercritical states. The hydrogen bonding structure and the diffusion coefficients in an ensemble of simulated states were previously analyzed and a good agreement with available experimental data was found. Dynamic properties of hydrogen bonding like the bond lifetimes and the influence of hydrogen bonds in the vibrational spectra are discussed along a range of simulation conditions. A nonlinear behavior of the hydrogen-bond lifetime as a function of temperature is observed in subcritical water whereas a linear dependence is found in supercritical water. Special attention is paid to the intermolecular vibrational spectrum (10–400 cm^{-1}). It has been observed that the mode centered at 200 cm^{-1}, attributed to the intermolecular O—O stretching vibration in the ambient state remains active in the supercritical states.

PACS number(s): 61.20.Ja, 61.25.Em, 78.30.−j, 78.30.Cp

I. INTRODUCTION

In recent years supercritical fluids have earned the increasing interest of the scientific community because of their singular physical and chemical properties and their use in chemical industry and materials physics [1]. Supercritical water (SW) plays an important role in the oxidation of organic compounds, in the pharmaceutical industry and as process water in some power generating complexes. Nevertheless, the detailed microscopical picture of SW has not been completed yet. Experimental data available show some significant discrepancies concerning the structure of SW and a controversy arose about the existence of hydrogen bonds (HB) in water at supercritical conditions. The main problem is the determination of the oxygen-hydrogen and hydrogen-hydrogen partial radial distribution functions $g_{OH}(r)$ and $g_{HH}(r)$. Botti *et al.* [2] have used a neutron-diffraction technique which allows the measurement of these partial distribution functions by means of samples containing mixtures of light water, heavy water, and HDO. They measured the differential cross section for each sample and extracted the partial radial distribution functions.

On the other hand, Bellissent-Funel and co-workers [3,4] have measured the neutron-weighted radial distribution function $g(r)$ for heavy water and have employed a decomposition procedure to obtain the three partial atomic contributions. Nevertheless, at short distances ($r<3$ Å) there is an important phase opposition between the oxygen-hydrogen and the hydrogen-hydrogen functions and the decomposition becomes delicate. The interpretation of both groups of data has generated contradictory conclusions and actually there is not a unique picture of the HB structure of SW from the experimental neutron-scattering point of view. Other techniques like nuclear magnetic resonance [5], infrared (IR) absorption, and x-ray scattering [6] have supported a significant presence of hydrogen bonding in SW. However, the question about the *degree* of H bonding is still open. Hoffmann and Conradi [7] tried to answer that question by means of proton chemical shift measurements and included a detailed comparison of experimental and theoretical results. On the other hand, the dynamic information of SW at the microscopical level is much more scarce in the literature and it basically consists of diffusion coefficient measurements by Lamb *et al.* [8] and spectroscopic data obtained by Franck and Roth [9] and by Ricci *et al.* [10].

The theoretical investigations on SW are mainly based on computational results obtained via Monte Carlo and molecular-dynamics (MD) simulations. A variety of potential models has been employed: TIP4P [11], rigid SPC and its variations [12–17] or flexible SPC models [18–20]. The HB definition employed has been established as a factor which has a relevant influence on the computed results [20,21]. Most of the classical computer simulation studies have reported a significant amount of hydrogen-bonding in SW. Nevertheless, Fois *et al.* [22] employed the Car-Parrinello *ab initio* MD method to investigate microscopical properties of SW at 730 K and obtained a low amount of HB. The structure of SW which arises from most of these calculations is formed by a relevant amount of hydrogen bonds and it has lost the tetrahedral configuration typical of ambient conditions. However, supercritical states have a degree of HB connectivity large enough to, in our opinion, still talk about HB *networks* in SW. The networks are mainly formed by chains of H-bonded waters which have ramifications and are mutually interconnected. This idea will be developed in Sec. IV B. In a previous work [20], a detailed structural analysis showed the presence of cavities and long H-bonded chains in SW at moderate temperatures around 573–673 K with densities higher than 0.5 g/cm^3.

It is interesting to point out that few works [18,19] have analyzed dynamic properties of the HB networks in SW such as the HB lifetimes, the intramolecular vibrational spectrum

*Permanent address.

TABLE I. Simulated thermodynamic states. The states 1–4 are located in the experimental liquid-vapor coexistence curve and states 5–9 belong to the supercritical region of the experimental phase diagram. The averaged molecular dipole moments $\langle \mu \rangle$ (in Debye) have an estimated error of about of 0.01 *D*.

State	Temperature (K)	Density (g/ cm^3)	$\langle \mu \rangle$ (D)
1	298	1.00	2.44
2	350	0.97	2.44
3	403	0.91	2.44
4	523	0.75	2.44
5	573	0.83	2.28
6	673	0.49	2.20
7	673	0.66	2.27
8	673	0.83	2.21
9	773	0.83	2.20

(connected with the mid-IR spectrum) or the intermolecular vibrational spectrum (connected with the far-IR and the Raman low-frequency spectrum). The study of those kind of properties under thermodynamic changes in SW is the main objective of the present work. We have used a flexible SPC water model especially adapted for SW states as detailed in Sec. II. The paper is organized in the following way: First we report the computational details and the potential model employed. The description of the HB definition assumed is sketched in Sec. III. A comparison between the structure of SW derived from our model and very recent experimental data is also presented, including a discussion of the HB populations in the SW states considered. The study of the persistence time of HB in SW is performed as a function of temperature and density, obtaining a qualitative description of the temperature dependence in supercritical states and comparing it with that of states on the liquid-vapor coexistence curve. Finally, a detailed analysis of the inter- and intramolecular vibrational spectra of SW is reported and the physical interpretation of the intermolecular vibrational modes is discussed.

II. COMPUTATIONAL DETAILS

We performed MD simulations of 216 flexible SPC-water molecules at four temperatures along the experimental liquid-vapor coexistence curve [23]. It should be pointed out that the liquid-vapor coexistence curve corresponding to the SPC model does not coincide with that of real water [24]. We have also simulated five thermodynamic states located on the experimental supercritical region [25]. The characteristics of the simulated states are reported in Table I.

The SPC interaction potential [26], which consists of three interaction sites located at the atomic positions, has been assumed to model intermolecular forces. In addition, intramolecular interactions were included, according to the potential of Toukan and Rahman [27], but with slightly different potential parameters. That reparametrized model [28] satisfactorily reproduces the main trends of the IR spectrum of water [29] in ambient conditions. Furthermore, our preliminary investigations showed that the supercritical states generated with such model are unstable. To surmount that problem the adjustment of the value of the molecular dipole moment of water (which has an averaged value of 2.44 Debye in room conditions for our model), to appropriate values for each supercritical state was required. This adjustment was performed though the modification of the effective charges of hydrogens and oxygens, and produced the molecular dipole moments listed in Table I. It should be noted that the rigid version of the SPC potential has a fixed molecular dipole moment of 2.27 Debye that does not require the adjustment in the equilibration process of the supercritical states [20].

We considered periodic boundary conditions and the Ewald sum rule [30] was employed in order to compute the long-ranged Coulombic interactions. A leap-frog Verlet integration algorithm with coupling to a thermal bath was used [31]. The integration time step was 0.5 fs. The equilibration of the translational and internal degrees of freedom was performed independently [32] with the aim to drive quickly the system to fluctuate around the desired temperature. Static and dynamic properties for each simulation were evaluated from MD runs of 150 ps after an equilibration period of 20 ps for coexistence curve states and 100 ps for supercritical states.

TABLE II. Mean number of HB per molecule $\langle n \rangle$ as a function of the HB definition. Estimated uncertainties are of about 0.1% for each value.

State	Energetic def.	Geometrical def.	Experiment [5]
1	3.5	3.7	3.9
5	0.9	1.6	1.6
6	1.3	2.1	2.0

III. HYDROGEN BOND DEFINITION

The adoption of a criterion to decide that two molecules are hydrogen-bonded is a delicate task, since the water pair energy is described by means of a continuous potential model. In a previous work [20], we investigated the influence of the HB definition on the structure of supercritical water. The main conclusion was the excellent agreement for the averaged number of HB per molecule between the MD results with the flexible SPC model and the experimental data reported in Ref. [5] when a pure geometrical criterion is used. The comparison between geometrical and energetic definitions is sketched in Table II for a few selected states. See Ref. [20] for more details. Moreover, the same kind of definition has proved to be useful to model HB in liquid-vapor coexistence curve MD simulations [33]. Therefore, we have used in this work the same geometrical convention of Refs. [20] and [33]: Two water molecules are linked by one HB when three conditions are fulfilled:

(1) The distance R_{OO} between the oxygens of both molecules is smaller than R_{OO}^{c}.

(2) The distance R_{OH} between the oxygen of the acceptor molecule and the hydrogen of the donor is less than R_{OH}^{c}.

(3) The bond angle ϕ between the O—O direction and the molecular O—H direction of the donor, where H is the hydrogen which forms the bond, has to be less than ϕ^{c}.

These cutoff values are given by the first minima of the partial oxygen-oxygen and oxygen-hydrogen radial distribu-

tion functions [20]: $R_{OO}^{c}=3.6$ Å for subcritical water states, $R_{OO}^{c}=4.6$ Å for supercritical states, $R_{OH}^{c}=2.4$ Å and $\phi^{c}=30°$ for all states.

Perhaps the main advantage of the use of the geometrical instead of the energetic definition is that we can identify the H and O atoms which participate in each single HB. This allows us to classify oxygen and hydrogen atoms into several groups. The oxygens have been separated according to the number of HB in which they participate. We have also distinguished between bonded and nonbonded hydrogens.

IV. SIMULATION RESULTS AND DISCUSSION

Structural and dynamic properties of supercritical water states as a function of the thermodynamic conditions are reported: We start discussing the most recent experimental neutron-diffraction results and analyze the hydrogen bond lifetimes, compared to states on the liquid-vapor coexistence curve. A different temperature dependence of the HB lifetime is found for sub- and supercritical states. The far- and mid-infrared spectra of SW are studied through the calculation of the spectral densities corresponding to the velocity and the relative velocity fluctuation autocorrelation functions and a physical interpretation of the most relevant features of the spectra is sketched.

A. Structure

We have previously tested the ability of the flexible SPC model to reproduce the microscopic structure and self-diffusion coefficient of SW for a wide range of states [20], comparing the computational structure with the data from Soper *et al.* [34] and obtaining a general good agreement, which is particularly remarkable for the state at 573 K and 0.72 g/cm^3.

Nevertheless, it must be pointed out that we compared computed and experimental partial radial distribution functions, whereas usually the information directly available to experimentalists is the total structure factor $S(k)$ or, analogously, the total neutron-weighted radial distribution function $g(r)$ [35]. The procedure to find the partial $g(r)$ is based on the decomposition of the total function in three contributions according to the neutron-scattering lengths. In the case of water [36]:

$$g(r)=0.092g_{OO}(r)+0.422g_{OH}(r)+0.486g_{HH}(r). \quad (1)$$

This was the procedure followed by Bellissent-Funel *et al.* [3,4]. However, Botti *et al.* [2] recently argued that the total $g(r)$ is not sensitive to the behavior of the $g_{OH}(r)$ and $g_{HH}(r)$ at short distances, because of the almost exact phase opposition of the two latter functions. They improved old experiments [37,38] performed with an isotopic mixture technique which allows the obtention of the three partial radial distribution functions, and reconstructed the neutron-weighted $g(r)$. There is a good agreement between both experimental groups about the total $g(r)$ for supercritical water, although they disagree about the short distance ($r<3$ Å) behavior of $g_{OH}(r)$ and $g_{HH}(r)$. The importance of the partial radial distribution functions and, especially of their short distance profile, is due to the fact that these functions are directly related to the presence of HB: The first peak of $g_{OH}(r)$ is the HB signature. We have considered the comparison between the experimental and the simulated neutron-weighted $g(r)$ as a test of our model.

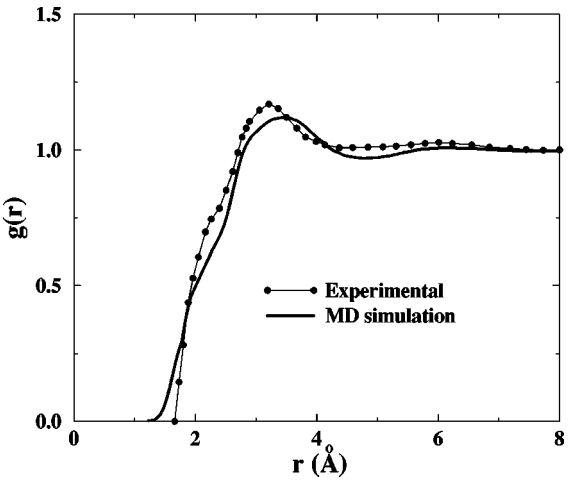

FIG. 1. Total radial distribution function comparison at 673 K. The experimental density is $\rho=0.58$ g/cm^3 and the simulated density is $\rho=0.66$ g/cm^3.

We calculated the total radial distribution function at 673 K and 0.66 g/cm^3 and we compared it with the neutron-diffraction data of Botti *et al.* [2], as shown in Fig. 1. We observe a good qualitative agreement between both functions, although it must be noted the slightly different densities considered (the experimental density is 0.58 g/cm^3 whereas the density of the simulated state is 0.66 g/cm^3). Nevertheless, this is not a relevant issue, since the variations in the microscopical structure due to changes in the density of the system are very small and can be neglected [20].

B. H-bond populations

The mean number of HB per molecule $\langle n\rangle$ in the simulated states and the averaged HB rates n_i (the percentage of waters forming i HB) are presented in Table III. Subcritical states show similar percentages of HB molecules to those of SW states at ''high'' density (0.83 g/cm^3), whereas the ''low'' density SW states present a weaker HB structure, i.e., lower $\langle n\rangle$.

The results found by MD simulation indicate two main features: First of all, the persistence of a remarkable population of HB in SW at temperatures between 573 and 773 K,

TABLE III. Percentages of waters forming i HB (n_i) and averaged number of HB per water molecule ($\langle n\rangle$) for several states of Table I. Estimated uncertainties are about 0.1 for each value.

State	n_0	n_1	n_2	n_3	n_4	n_5	n_6	$\langle n\rangle$
1	<0.1	0.3	4.8	26.0	58.2	10.2	0.5	3.7
3	0.5	5.6	23.0	38.9	28.6	3.1	0.3	3.0
4	3.2	17.6	36.0	30.7	11.4	1.0	0.1	2.3
5	1.9	12.0	29.3	33.4	18.2	4.5	0.7	2.7
6	16.1	33.9	31.2	14.3	3.8	0.6	0.1	1.6
7	7.0	24.0	34.2	23.6	9.0	1.9	0.3	2.1
8	3.4	16.1	31.1	29.2	15.0	4.4	0.8	2.5
9	4.7	17.9	31.2	27.8	13.9	4.0	0.5	2.4

for a density range from 0.5 g/cm^3 to higher values. The second relevant finding is the dominant presence of H-bonded chains in most of SW states, since the mean HB number is around two in all states considered. Moreover, since we have detected a significative amount of three-H-bonded waters in most of SW states, we can conclude that SW (at moderate temperatures) is basically organized in terms of chains of hydrogen-bonded molecules which allow ramifications. The complexity of these chains depends on both the temperature and density of the system. We can assume that some kind of HB network persists in SW. This picture of the SW microscopical structure is qualitatively different from the experimental interpretation [2] of the neutron-scattering data, based on the assumption that only residual HB remain in SW, mainly due to the presence of dimers. In our opinion, the main reason for the discrepancy could be associated to the difficulty of the interpretation of the neutron-diffraction results, although it could also due to shortcomings of the flexible SPC model used in this work.

C. HB lifetimes

The fast librational motions of water, which rearrange the HB network through the breaking and subsequent reformation of HB in short-time intervals, make difficult the study of the temporal evolution of the HB networks. Some results about the lifetimes of HB in water at ambient conditions [39,40] and for states on the liquid-vapor coexistence curve [33] have been reported previously, whereas only two works from the same group [18,19] have investigated the HB lifetimes in SW for temperatures ranging 773–1073 K.

A variety of HB lifetime definitions may be used [41]. We have employed the HB lifetime (or persistence time) definition previously used by Rapaport [39] and Matsumoto and Gubbins [42]. We define a variable $\eta_{nm}(t)$ that takes binary values depending on the HB state of a pair of molecules:

$$\eta_{nm}(t)=\begin{cases}1, & \text{if molecules } n \text{ and } m \text{ are H bonded}\\ 0, & \text{otherwise.}\end{cases} \tag{2}$$

The normalized autocorrelation function of $\eta_{nm}(t)$ is defined by

$$C^i_\eta(t)\equiv\frac{\langle \eta_{nm}(0)\,\eta_{nm}(t)\rangle}{\langle \eta^2_{nm}(0)\rangle}. \tag{3}$$

This function gives the probability that the HB existing between molecules m and n at the instant $t=0$ persists at the instant t, independently of its evolution in that time interval. Consequently, that correlation function allows the breaking and reformation of HB in a given time period, although it does not consider collective processes like the *switching allegiance* [43] of water molecules which modify the topology of the HB network. $C^i_\eta(t)$ is called the *intermittent lifetime autocorrelation function*. The $C^i_\eta(t)$ found for states 1–4 were reported previously [33], whereas the correlation functions obtained for the SW states 5, 8, and 9 are shown in Fig. 2. We assume an exponential relaxation behavior for short times (this hypothesis will be tested below), although we must distinguish between two time domains: The intervals [0,0.05] ps (fast decay) and [0.05,0.5] ps (slow decay). According to the exponential decay approximation, we can calculate the *intermittent lifetime* $\tau^i_{\rm HB}$ by

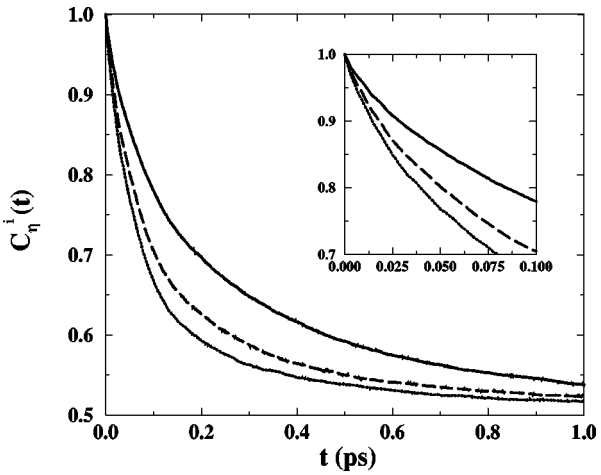

FIG. 2. Intermittent HB lifetime autocorrelation function in supercritical conditions at the density of 0.83 g/cm^3: 573 K (continuous line), 673 K (dashed line), and 773 K (dotted line). Detail of short times in the inset.

$$C^i_\eta(t)\cong\exp\left\{-\frac{t}{\tau^i_{\rm HB}}\right\}. \tag{4}$$

We also considered another possibility: If $\eta_{nm}(t)$ is fixed to zero after the first breaking of the HB between molecules n and m, we will be able to estimate the time associated to the librational motions of water. The corresponding autocorrelation function $C^c_\eta(t)$ is the *continuous lifetime autocorrelation function* and $\tau^c_{\rm HB}$ is called the *continuous lifetime*. We present $C^c_\eta(t)$ for the same states as $C^i_\eta(t)$ in Fig. 3. We have included a semilog plot in the range of short times in order to check the exponential approximation, which is basically fulfilled, in the range of short times. Here we note that the decay times are lower than the analogous times corresponding to the intermittent correlation function.

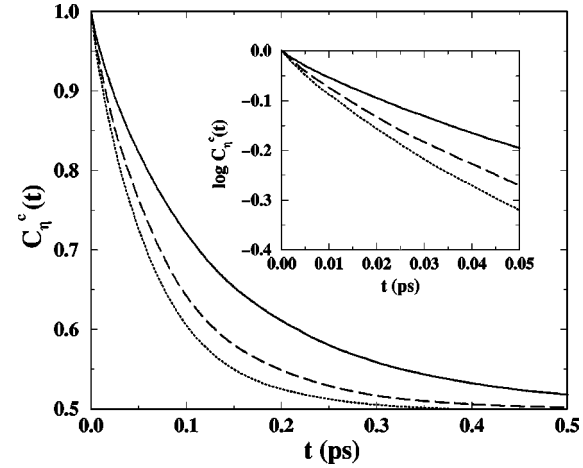

FIG. 3. Continuous HB lifetime autocorrelation function in supercritical conditions at 0.83 g/cm^3: 573 K (continuous line), 673 K (dashed line), and 773 K (dotted line). The inset shows the exponential decay approximation for short times [note we present $\ln C^c_\eta(t)$ instead of $C^c_\eta(t)$].

TABLE IV. Intermittent and continuous hydrogen bond persistence time at different thermodynamic states. The estimated errors are lower than 5% of each value.

State	τ^i_{HB}	τ^c_{HB}
1	2.56	0.53
2	1.82	0.47
3	1.63	0.41
4	1.27	0.34
5	0.49	0.20
6	0.35	0.15
7	0.36	0.16
8	0.34	0.14
9	0.27	0.13

HB lifetimes are summarized in Table IV. It is important to remark that MD calculations can only provide approximate values of HB persistence times, since the exponential regression adopted to estimate the lifetimes include some arbitrariness related to the time interval considered. The persistence times obtained from $C^i_\eta(t)$ in the time interval of [0,0.05] ps are equivalent to those obtained from $C^c_\eta(t)$ in the same time interval. The intermittent lifetimes are about four times larger than the continuous ones for subcritical states and about twice for SW.

Depolarized Rayleigh scattering has been traditionally used to obtain experimental information on the HB lifetimes [36,44]. It is important to remark that these experimental values cannot be directly associated with the intermittent or continuous lifetimes. The experimental result at 298 K ($\tau = 0.5$ ps) is in qualitative agreement with our results although the experimental changes with temperature were markedly bigger than those in our MD simulations [36,44]. Nevertheless, the different temperature interval studied in experiments (260–350 K) should be noted. Other MD studies with different potential models and methods [39,40,45–47] obtained a variety of values at ambient conditions which, in general, are of the order of magnitude of 1 ps.

The temperature dependence of intermittent and continuous HB lifetimes in SW is studied in Fig. 4. We compare SW lifetimes for states at constant density with the lifetimes obtained for subcritical states, which correspond to systems with different temperature and density. A relevant fact is the qualitatively different dependence of τ_{HB} for both classes: We observe a nonlinear decreasing of τ^i_{HB} for the states lying on the liquid-vapor coexistence curve, whereas a monotonic behavior is found for SW states. One possible reason of that different behavior could be the fact that the states on the coexistence curve are not at the same density: The nonlinear behavior would be associated to variations of the density of the system.

Concerning τ^c_{HB}, we observe a linear decreasing with increasing temperature for subcritical states whereas the variation for supercritical states is very small, with a tendency to decrease with increasing temperature. On the other hand, at 673 K we cannot observe noticeable changes for densities between 0.49 and 0.83 g/cm^3 (see Table IV). This fact must be associated to the temperature and density range studied, since in the high-temperature range Mizan *et al.* [18,19] observed a linear decreasing with increasing temperature and also a linear decreasing with increasing density for the continuous lifetime.

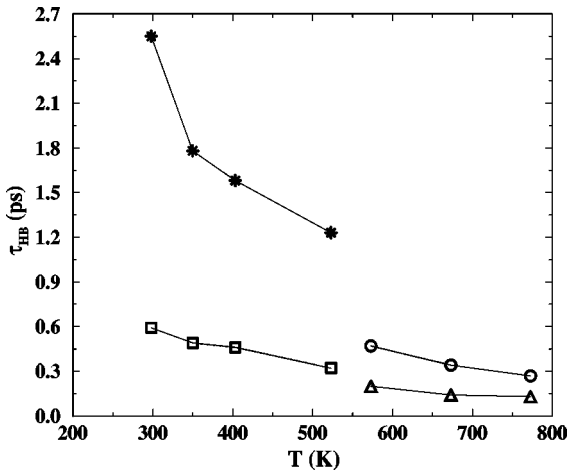

FIG. 4. Temperature dependence of the HB lifetime for sub- and supercritical states: Stars and circles account for the intermittent lifetime, whereas squares and triangles correspond to the continuous lifetime (the state at 673 K is state 8).

D. Atomic spectral densities

1. Hydrogens

In a previous work [20] we analyzed the real part of the spectral densities $S(\omega)$ associated with the atomic velocity autocorrelation functions and given by

$$S(\omega) = \int_0^\infty dt \langle \mathbf{v}(0) \cdot \mathbf{v}(t) \rangle \exp\{-i\omega t\}, \tag{5}$$

at different thermodynamic conditions in SW. The calculation of the $S(\omega)$ was done by numerical integration using a Bode rule. A Hanning window was previously applied to the velocity autocorrelation functions of Eq. (5). The main motivation of this spectral analysis was a recent work of Ricci *et al.* [10] which reported light- and neutron-scattering results of SW, focused on the study of the OH stretching band. They employed a Q-dependent density of states that is equivalent to a hydrogen-projected density of states $g_H(\hbar\omega)$, which is a function directly corresponding to the hydrogen spectral density $S_H(\omega)$ [48]. We obtained a good agreement for the frequency band shift between gas and liquid phases for the OH stretching band. We also observed a deep connection between the displacements of the vibrational and rotational spectral bands and the HB populations, under joint temperature and density changes. Stretching and bending vibrations are, respectively, connected to forward and backward shifts when temperature increases and density decreases, due to the progressive destruction of the HB network. In an opposite way, the libration band displacement does not follow a clear pattern under joint thermodynamic variations. The study of the density and temperature dependence is necessary to interpretate the observed behavior of the libration band. Therefore, we have used Eq. (5) to calculate the spectral densities of several states of Table I.

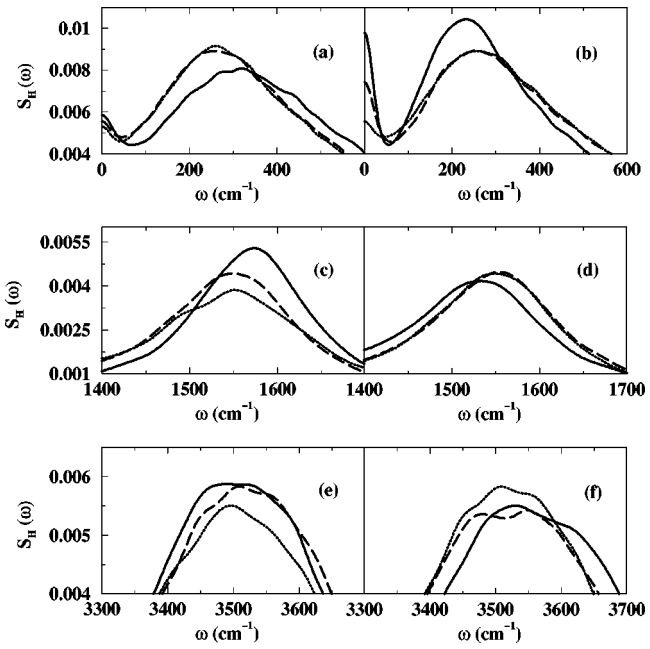

FIG. 5. Hydrogen spectral densities $S_H(\omega)$ (in arbitrary units). Libration band (a) and (b), bending band (c) and (d) and stretching band (e) and (f). Graphs (a), (c), and (e) correspond to the density of 0.83 g/cm^3: 573 K (continuous line), 673 K (dashed line), and 773 K (dotted line). Graphs (b), (d), and (f) correspond to 673 K: 0.49 g/cm^3 (continuous line), 0.66 g/cm^3 (dashed line), and 0.83 g/cm^3 (dotted line).

The analysis of the separate temperature and density influence on the spectral bands can be carried out from data presented in Fig. 5 and Table V. We have calculated the hydrogen spectral density $S_H(\omega)$ for states at 673 K and variable density as well as for states at the fixed density of 0.83 g/cm^{-1} and temperatures between 573 and 773 K. Moderated spectral shifts of the three spectral bands are observed under density variations [Figs. 5(b), 5(d), and 5(f)], whereas the influence of the temperature on the band maxima displacements is more relevant for librations [Fig. 5(a)] and bending [Fig. 5(c)] and negligible for stretching [Fig. 5(e)]. We also note that relative intensities and bandwidths remain basically unchanged, although these properties are again more sensitive to temperature changes than to density variations. We should mention here that the flexible SPC model that we have employed in our simulations is a pure classical potential and, since proton vibrations are properly quantum properties, we are only able to calculate accurately the frequencies of vibration or band shifts (thanks to the previous adjustment of the potential model [28]) and we can only consider the relative intensities of the spectral modes. Consequently, the results concerning intensities and bandwidths are only indications of the tendency to change under thermodynamic variations.

TABLE V. Frequency band maxima (in cm^{-1}) for the hydrogen spectral densities $S_H(\omega)$ of SW at different states. The uncertainties of the MD simulation values are about 1% of each value.

State	Libration	Bending	Stretching
5	320	1575	3500
6	225	1530	3545
7	260	1560	3515
8	255	1550	3510
9	260	1555	3495

The spectral band displacements can be attributed to two different and complementary effects: First, the variation of HB populations in each supercritical state (see Table III) and second, the different frequency maxima for bonded and nonbonded hydrogens in SW. We have obtained typical values of the librational band maximum about 450 cm^{-1} for bonded hydrogens and about 230 cm^{-1} for non-H-bonded atoms. The bending band maxima are about 1570 cm^{-1} for bonded hydrogens and 1540 cm^{-1} for nonbonded hydrogens, whereas the stretching band has peaks about 3450 cm^{-1} for bonded hydrogens and about 3620 cm^{-1} for the nonbonded atoms. We have summarized these values for the set of SW states since the variation of each value with the thermodynamic changes considered is only of about 3%. A similar behavior was detected for bonded and nonbonded molecules in subcritical water [33]. Consequently, the libration band is shifted to lower frequencies when temperature increases [Fig. 5(a)] due to the bigger amount of nonbonded hydrogens in that case. The density effect [Fig. 5(b)] is analogously explained: As density increases, the population of bonded hydrogens grows and, because of the higher libration frequency of the bonded hydrogens, the band shifts forward.

2. Oxygens

The spectral densities of the oxygen and of the molecular center-of-mass velocity autocorrelation functions are the properties commonly used to study the intermolecular vibrational motions, since they are connected to the far-IR and the low-frequency Raman spectrum of water [49,50]. The calculation of these functions revealed a weakening of the two prominent spectral bands of ambient water located at 60 and 200 cm^{-1} [51,52] when temperature increases in the liquid-water coexistence curve [33]. The 60 cm^{-1} band has been associated to the vibration frequency of a water molecule inside the cage formed by its closest neighbors [33] whereas the 200 cm^{-1} band is connected to the stretching vibration of the H-bonded O—O pairs [51]. We observe in Fig. 6 the virtual absence of these modes in SW: Only a weak trace of the shoulder centered at 200 cm^{-1} in the ambient state is observable for the SW states. The 60 cm^{-1} mode has absolutely vanished. We can assume the absence of the cage effect in SW because of the weakening of the HB network, but there is no clear reason for the absence of the band located around 200 cm^{-1} in the supercritical states, since it has been established (Table III) that there is a remarkable amount of H-bonding in SW. We need to perform a more detailed analysis by using an additional spectroscopic property (instead of the oxygen velocity autocorrelation function), namely the O—O relative velocity fluctuation, in order to discuss the point.

We have calculated the spectral density $S_O^{\Delta \mathbf{v}}(\omega)$ associated to the oxygen-oxygen relative velocity fluctuation $\Delta \mathbf{v}(t)$ autocorrelation function:

$$S_O^{\Delta \mathbf{v}}(\omega) = \int_0^\infty dt \langle \Delta \mathbf{v}(0) \cdot \Delta \mathbf{v}(t) \rangle \exp\{-i\omega t\} \qquad (6)$$

with

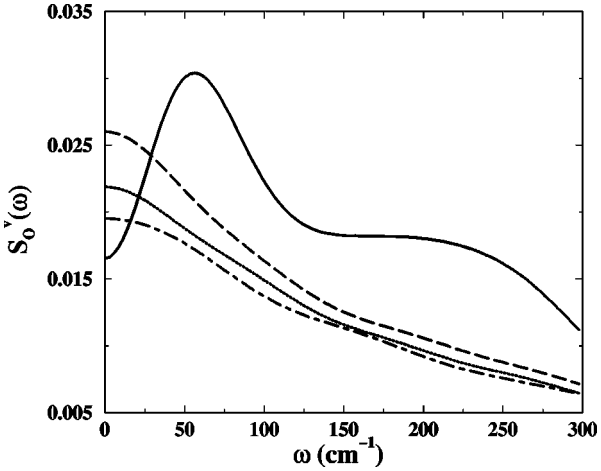

FIG. 6. Spectral densities $S_O(\omega)$ (in arbitrary units) in ambient and supercritical conditions: 298 K, 1 g/cm^3 (continuous line), 573 K, 0.83 g/cm^3 (dashed line), 673 K, 0.83 g/cm^3 (dotted line), and 773 K, 0.83 g/cm^3 (dot-dashed line). All functions have calculated for oxygens which form four HB.

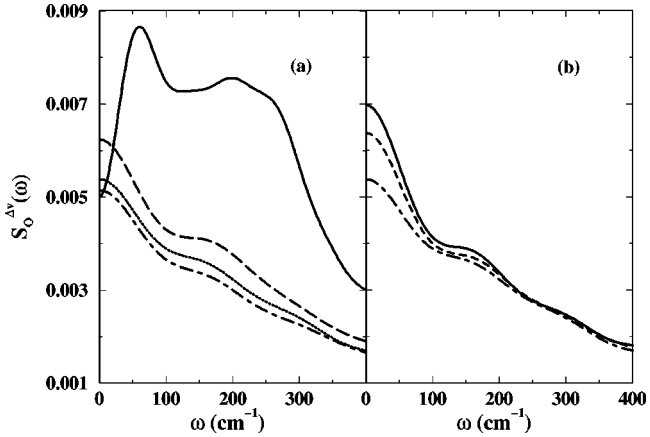

FIG. 7. Spectral densities $S_O^{\Delta \mathbf{v}}(\omega)$ (in arbitrary units). (a) Temperature dependence: 298 K, 1 g/cm^3 (continuous line), 573 K, 0.83 g/cm^3 (dashed line), 673 K, 0.83 g/cm^3 (dotted line), and 773 K, 0.83 g/cm^3 (dot-dashed line). (b) Density dependence at 673 K: 0.49 g/cm^3 (continuous line), 0.66 g/cm^3 (dashed line), and 0.83 g/cm^3 (dot-dashed line).

$$\Delta \mathbf{v}(t) \equiv \mathbf{v}_O(t) - \mathbf{v}_{O'}(t). \tag{7}$$

Here oxygens O and O′ are hydrogen bonded and obviously the relative velocity vector $\Delta \mathbf{v}(t)$ is directed along the line which crosses both oxygens of the H-bonded pair. Consequently, $S_O^{\Delta \mathbf{v}}(\omega)$ is a natural candidate as an O—O stretching detector. His efficiency is tested in Fig. 7. We obtain two prominent peaks in ambient conditions centered at 60 and 195 cm^{-1} and a shoulder for the SW states at temperatures between 573 and 773 K and constant density, approximately centered at 160 cm^{-1} [Fig. 7(a)]. The analysis of the density dependence [Fig. 7(b)] reveals again the presence of the shoulder around 160 cm^{-1}. We observe that it is not shifted with density changes (in the density range considered). In summary, SW dimers still have a O—O stretching motion that can be observed if we use appropriate tools.

V. CONCLUDING REMARKS

Microscopic structure and dynamic properties of supercritical water at different thermodynamic conditions have been analyzed through a series of MD simulations using a flexible SPC potential model. We have observed a good agreement for the neutron-weighted radial distribution function at 673 K when comparing to recent experimental data. The populations of HB reported in Table III are also in good agreement with available experimental measurements and indicate the breakdown of the tetrahedral H-bond structure typical of ambient liquid water in the SW states, although the amount of hydrogen bonded water molecules in supercritical conditions is still very relevant. The effect of the density variations has been found to be more important than the effect of temperature changes concerning the distribution of HB populations.

Lifetimes of HB are of the order of 1 ps in ambient water as well as for states on the liquid-vapor coexistence curve, in a qualitative good agreement with experimental data. The temperature dependence for the HB lifetime in these states follows a nonlinear behavior. In SW, HB lifetimes are significantly smaller than the former and their temperature dependence has been found to decrease monotonically. Furthermore, the persistence of HB in SW is approximately density independent in the density range studied.

We have calculated vibrational and librational frequencies of SW in a range of thermodynamic conditions. The comparison of the OH stretching liquid-vapor band shifts with available experimental data [10] was satisfactorily performed previously [20]. However, experimental information including bending and librational motions in SW is not available yet and it would be needed in order to test part of the dynamic information presented in this work and its interpretation. We suggest the measurement of the Raman and/or infrared spectra in the frequency range of less than 3000 wave numbers for SW.

The behavior of the OH stretching, the bending, and the librational bands in SW under different thermodynamic conditions is basically associated with the variation in the HB populations. However, the band shifts also depend on an additional factor: The frequency of librations and of the OH stretching vibration for H-bonded molecules in SW is markedly lower than the corresponding frequencies of nonbonded molecules. This double effect explains well the spectral band shifts of the frequency bands in SW under temperature and density changes.

The persistence of the O—O stretching vibration has been proven also in SW: Whereas the usually employed spectral density of the oxygen velocity autocorrelation function is not sensitive to the 200 cm^{-1} mode, we have observed its signature when analyzing the relative oxygen-oxygen velocity. Conversely, the low-frequency band centered at 60 cm^{-1} and related to the cage effect typical of dense liquids is totally absent in SW.

ACKNOWLEDGMENTS

The author is grateful to Alenka Luzar for fruitful comments and discussions. Financial support of the Generalitat de Catalunya, Project No. 19975GR-00149 and of the Ministerio de Educación y Ciencia (DGES), Project No. PB96-0170-C03-02 are also acknowledged.

[1] C. A. Eckert, B. L. Knutson, and P. G. Debenedetti, Nature (London) **383**, 313 (1996).
[2] A. Botti, F. Bruni, M. A. Ricci, and A. K. Soper, J. Chem. Phys. **109**, 3180 (1998).
[3] M.-C. Bellissent-Funel, T. Tassaing, H. Zhao, D. Beysens, B. Guillot, and Y. Guissani, J. Chem. Phys. **107**, 2942 (1997).
[4] T. Tassaing, M.-C. Bellissent-Funel, B. Guillot, and Y. Guissani, Europhys. Lett. **42**, 265 (1998).
[5] N. Matubayashi, C. Wakai, and M. Nakahara, J. Chem. Phys. **107**, 9133 (1997).
[6] Yu. E. Gorbaty and A. G. Kalinichev, J. Phys. Chem. **99**, 5336 (1995).
[7] M. M. Hoffmann and M. S. Conradi, J. Am. Chem. Soc. **119**, 3811 (1997).
[8] W. J. Lamb, G. A. Hoffman, and J. Jonas, J. Chem. Phys. **74**, 6875 (1981).
[9] E. U. Franck and K. Roth, Faraday Discuss. Chem. Soc. **43**, 108 (1967).
[10] M. A. Ricci, M. Nardone, A. Fontana, C. Andreani, and W. Hahn, J. Chem. Phys. **108**, 450 (1998).
[11] R. D. Mountain, J. Chem. Phys. **90**, 1866 (1989).
[12] P. T. Cummings, H. D. Cochran, J. M. Simonson, R. E. Mesmer, and S. Karaborni, J. Chem. Phys. **94**, 5606 (1991).
[13] A. A. Chialvo and P. T. Cummings, J. Chem. Phys. **101**, 4466 (1994).
[14] P. T. Cummings and A. A. Chialvo, J. Phys.: Condens. Matter **8**, 9281 (1996).
[15] A. A. Chialvo, J. Chem. Phys. **104**, 5240 (1996).
[16] A. A. Chialvo and P. T. Cummings, J. Chem. Phys. **105**, 8274 (1996).
[17] A. A. Chialvo, P. T. Cummings, J. M. Simonson, and R. E. Mesmer, J. Mol. Liq. **73-74**, 361 (1997).
[18] T. I. Mizan, P. E. Savage, and R. M. Ziff, J. Phys. Chem. **100**, 403 (1996).
[19] T. I. Mizan, P. E. Savage, and R. M. Ziff, J. Comput. Chem. **17**, 1757 (1996).
[20] J. Martí, J. Chem. Phys. **110**, 6876 (1999).
[21] A. G. Kalinichev and J. D. Bass, J. Phys. Chem. A **101**, 9720 (1997).
[22] E. S. Fois, M. Sprik, and M. Parrinello, Chem. Phys. Lett. **223**, 411 (1994).
[23] J. H. Keenan and F. G. Keyes, *Thermodynamic Properties of Steam* (Wiley, New York, 1937).
[24] J. J. de Pablo, J. M. Prausnitz, H. J. Strauch, and P. T. Cummings, J. Chem. Phys. **93**, 7355 (1990).
[25] The values of the critical point of experimental water are $T=647$ K$\rho=0.32$ g/cm^3 and $P=221$ bar, see, for instance [37].
[26] H. J. C. Berendsen, J. P. M. Postma, W. F. van Gunsteren, and J. Hermans, in *Intermolecular Forces*, edited by B. Pullman (Reidel, Dordrecht, 1981).
[27] K. Toukan and A. Rahman, Phys. Rev. B **31**, 2643 (1985).
[28] J. Martí, J. A. Padró, and E. Guàrdia, J. Mol. Liq. **62**, 17 (1994).
[29] J. Martí, E. Guàrdia, and J. A. Padró, J. Chem. Phys. **101**, 10 883 (1994).
[30] M. P. Allen and D. J. Tildesley, *Computer Simulation of Liquids* (Clarendon, Oxford, 1987).
[31] H. J. C. Berendsen, J. P. M. Postma, W. F. van Gunsteren, A. DiNola, and J. R. Haak, J. Phys. Chem. **81**, 3684 (1984).
[32] A. Wallqvist and O. Teleman, Mol. Phys. **74**, 515 (1991).
[33] J. Martí, J. A. Padró, and E. Guàrdia, J. Chem. Phys. **105**, 639 (1996).
[34] A. K. Soper, F. Bruni, and M. A. Ricci, J. Chem. Phys. **106**, 247 (1997).
[35] D. Chandler, *Introduction to Modern Statistical Mechanics* (Oxford University Press, New York, 1987).
[36] S. H. Chen and J. Teixeira, Adv. Chem. Phys. **64**, 1 (1986).
[37] P. Postorino, R. H. Tromp, M. A. Ricci, A. K. Soper, and G. W. Neilson, Nature (London) **366**, 668 (1993).
[38] R. H. Tromp, P. Postorino, G. W. Neilson, M. A. Ricci, and A. K. Soper, J. Chem. Phys. **101**, 6210 (1994).
[39] D. C. Rapaport, Mol. Phys. **50**, 1151 (1983).
[40] A. Geiger, P. Mausbach, J. Schnitker, R. L. Blumberg, and H. E. Stanley, J. Phys. (Paris), Colloq. **45**, C7-13 (1984).
[41] F. H. Stillinger, Adv. Chem. Phys. **31**, 1 (1975).
[42] M. Matsumoto and K. E. Gubbins, J. Chem. Phys. **93**, 1981 (1990).
[43] A. Luzar, Faraday Discuss. Chem. Soc. **103**, 29 (1996).
[44] D. Bertolini, M. Cassettari, M. Ferrario, P. Grigolini, and G. Salvetti, Adv. Chem. Phys. **62**, 277 (1985).
[45] A. Luzar and D. Chandler, J. Chem. Phys. **98**, 8160 (1993).
[46] D. Zichi and P. J. Rossky, J. Chem. Phys. **84**, 2814 (1986).
[47] F. Sciortino and S. L. Fornili, J. Chem. Phys. **90**, 2786 (1989).
[48] S. H. Chen and S. Yip, Phys. Today **29** (4), 32 (1976).
[49] R. W. Impey, P. A. Madden, and I. R. McDonald, Mol. Phys. **46**, 513 (1982).
[50] J. Martí, J. A. Padró, and E. Guàrdia, Mol. Simul. **11**, 321 (1993).
[51] G. E. Walrafen, in *Water: A Comprehensive Treatise*, edited by F. Franks (Plenum, New York, 1972), Chap. 5, Vol. 1.
[52] J. B. Hasted, S. K. Husain, F. A. M. Frescura, and J. R. Birch, Chem. Phys. Lett. **118**, 622 (1985).